Fractal and Morlet-wavelet analyses of M ≥ 6 earthquakes in the South-North Seismic Belt, China

Jeen-Hwa Wang[1, *], Kou-Cheng Chen[1], and Kao-Hao Chang[2]

[1] Institute of Earth Sciences, Academia Sinica, Taipei City, Taiwan
[2] Department of Civil Engineering, Chung Yuan Christian University, Taoyuan City, Taiwan

ABSTRACT

The M ≥ 6 earthquakes occurred in the South-North Seismic Belt, Mainland China (longitudes from 98 - 107°E and latitudes from 21 - 41°N) during 1900 - 2016 are taken to measure the multifractal dimensionsspatial distribution and time sequence of events and the dominant periods. The multifractal dimensions, D_q, are measured from the log-log plots of $C_q(r)$ versus r and $C_q(t)$ versus t, where $C_q(r)$ and $C_q(t)$ are the generalized correlation integrals for the epicentral distribution and time sequence of events, respectively. r and t are the epicentral distance and inter-event time, respectively, at positive q. The log-log plot of $C_q(r)$ versus r shows a linear portion when $\log(r_l) \le \log(r) \le \log(r_u)$. The r_l and r_u values are, respectively, 120 and 560 km for M ≥ 6 events, 100 and 560 km for M ≥ 6.5 events, and 63 and 560 km for M ≥ 7 events. The r_l value decreases with the lower-bound magnitude. D_q monotonically decreases with increasing q. The D_q values are between 1.618 and 1.426 for M ≥ 6 events, between 1.562 and 1.108 for M ≥ 6.5 events, and between 1.365 and 0.841 for M ≥ 7 events. The log-log plot of $C_q(t)$ versus t show a linear distribution when $\log(t_l) \le \log(t) \le \log(t_u)$, where t_l and t_u are, respectively, 5 and 50.1 years for M ≥ 6 events, 5 and 50.1 years for M ≥ 6.5 events, and 16 and 63.1 years for M ≥ 7 event, thus suggesting that the time sequences of earthquake in the study region are multifractal. The D_q values are between 0.830 and 0.703 for M ≥ 6 events, between 0.835 and 0.820 for M ≥ 6.5 events, and between 0.786 and 0.685 for M ≥ 7 events. The Morlet wavelet technique is applied to analyze the dominant periods of temporal variations in numbers of yearly earthquakes for the three magnitude ranges, i.e., M ≥ 6, M ≥ 6.5, and M ≥ 7. The resultant dominant period is 2.94 years for M ≥ 6 events and cannot be evaluated for M ≥ 6.5 and M ≥ 7 events.

1. INTRODUCTION

In 1944, the frequency-magnitude relation found by Gutenberg and Richter (1944) is the first scaling law to represent self-similarity of earthquake phenomena (Chen and Koyama 1995; Main 1996; Wang 1988, 2008; Wang et al. 2015). Current studies also lead to that self-similarity or scale-invariance is a common property of natural phenomena. Mandelbrot (1983) proposed the fractal geometry with fractal dimension to describe the scale-invariant natural phenomena. This concept has been applied to seismology (Turcotte 1989; Korvin 1992), including the fault properties (Aviles et al. 1987; Okubo and Aki 1987; Lee and Schwarcz 1995; Candela et al. 2012), the spatial distribution of earthquakes (Hirabayashi et al. 1992; Turcotte 1997; Wang and Shen 1999), the temporal variation in earthquakes (Smalley et al. 1987; Hirata 1989; Kagan and Jackson 1991; Ogata and Abe 1991; Papadopoulos and Dedousis 1992; Koyama et al. 1995; Wang and Lee 1995, 1997; Wang 1996a; Kagan 2007; Michas et al. 2014), and earthquake ruptures (Wang 1995, 1996b; Aochi and Ide 2004; Ide and Aochi 2005, 2014; Manighetti et al. 2005; Lee et al. 2016).

A positive relation between the b-value of the frequency-magnitude law proposed by Gutenberg and Richter (1944) and the D value, which is the fractal dimension as described below, were: D = 3b/c (c = 1.5) by Aki (1982); b = D/3 by Turcotte (1986a); and b = D/2 by Turcotte (1986b).

* Corresponding author
　E-mail: jhwang@earth.sinica.edu.tw

However, Hirata (1989) reported a negative correlation between the two parameters for earthquakes in Japan. He also argued the positive relation given by Aki as mentioned above. From simulation results based on the 1-D dynamic spring-slider model, Wang (1991) found weak dependence of the b-value upon the D value. This conclusion is different from the theoretical postulation made by Aki (1982) and Turcotte (1986a, b) and from the observations (Hirata 1989). A possible reason for the difference might be that the D value used by Wang (1991) concerns the distribution of the fault breaking strengths while the D value used by the others is related to the fault geometry. Wang and Lin (1993) and Wang and Lee (1997) observed that the D value is negatively correlated with the b-value as pointed out by Hirata (1989). Hence, in order to understand the fractal characteristics of spatial distribution and temporal variation in earthquakes it is significant to study the fractal properties of seismicity.

It is important to explore the dominant recurrence periods in an earthquake sequence not only for earthquake physics but also for seismic hazard assessment. Although Fourier analysis is commonly applied to evaluate the dominant periods (or frequency) of a time series, it cannot provide the temporal variations in the dominant periods. The wavelet transform can be used to analyze time series that contain non-stationary power at many different frequencies (Daubechies 1990). In this study, the wavelet analysis (Combes et al. 1989; Pyrak-Nolte and Nolte 1995), also known as the multi-resolution analysis, is taken into account. For this technique a series of scaled and delayed oscillatory functions are used to decompose a time-varying signal into its non-stationary spectral components. Hence, the key advantage of wavelet analysis over traditional Fourier analysis is that the wavelet analysis provides information on how the spectral content varies with time delay. Wavelets are also advantageous over so-called windowed Fourier methods because with wavelets the relative accuracy of the delay and frequency remain constants cover all of the delay-frequency parameter space. The wavelet analysis application to geophysical problems can be seen in Torrence and Compo (1998). Here, a non-orthonormal Morlet wavelet analysis (Morlet et al. 1982; Chen et al. 2015) is taken into account.

Active orogeny due to the collision between the Indian and Eurasian plates (Molnar and Tapponnier 1975; Tapponnier and Molnar 1977; Tapponnier et al. 1982, 2001; Avouac and Tapponnier 1993; Royden et al. 2008) causes complex geological features and high seismicity in Mainland China. Complex geological conditions result in a non-uniform temporal-spatial distribution of earthquakes (Xu and Shen 1981; Huan and Shi 1987; Tan et al. 1987; Wang and Zhong 1987; Chen et al. 1994). Ma et al. (1992) delineated three highly seismic belts in Mainland China. The first is the South-North Seismic Belt (SNSB), with longitudes from 98 - 107°E and latitudes from 21 - 41°N, in the middle part of Mainland China. The earthquakes occurring in the SNSB should be inter-plate events. Historically, numerous large earthquakes occurred in the region. For example, two M ≥ 6 destructive earthquakes were located in the SNSB, i.e., the 3 February 1996 M 6.6 Lijiang earthquake, Yunnan (YSB 1998) and the 12 May 2008 M 7.9 Wenchung earthquake (Cheng et al. 2009; Zhang et al. 2009). The two events caused severe damage in the respective areas. Seismic hazard assessment is obviously an important issue in the region. Fractal analyses of spatial distribution of earthquakes will lead to geometric structures of earthquakes associated with active faults. Fractal and Morlet-wavelet analysesof earthquake sequence will provide the temporal characteristics and predominant recurrence periods for earthquakes. Active fault geometrical structures and earthquake recurrence times will influence the seismic hazard potential in a region. The present studies are helpful for understanding seismic hazards in the study region.

For the M ≥ 6 earthquakes that occurred from 1900 to 1990 in the region, Wang and Lee (1997) measured multifractal dimensions of earthquake sequence and Wang and Shen (1999) measured the multifractal dimensions of epicentral distributions. For the M ≥ 6 earthquakes that occurred in the region during 1901 - 2008, Wang (2013) studied the memory effect in the earthquake magnitude sequences and inter-event time using the fluctuation analysis technique. The calculated results show that the exponents of scaling law offluctuation versus window length are less than 0.5 for the earthquake magnitude sequences and inter-event time. Together with all kinds of given information, he concluded that the earthquakes are short-term correlated, in other words, the short-term memory effect is operative.

After 1990, numerous M ≥ 6 earthquakes occurred in the region. Hence, it is significant to re-investigate the multifractal properties of spatial distribution and earthquake sequence for M ≥ 6 earthquakes that occurred over a longer time period from 1900 to 2016. In addition, the Morlet wavelet analysis will also be taken to analyze the dominant earthquake sequence period.

2. DATA

A complete catalogue is needed to study the properties of earthquake temporal variation, especially for that made from instrumentally-recorded data. The earliest documented earthquake and damage data in Mainland China were found in 780 B.C. (ASIG 1975). Li (1960) compiled the first catalogue of Chinese earthquakes. Several Chinese earthquake catalogues were compiled by Chinese and foreign seismologists. Some of them were completed before 1978 and described by Lee et al. (1978). Ku (1983a, b) compiled a catalogue for earthquakes occurring from 1831 B.C. to 1979 A.D. Hsieh et al. (1989) compiled a catalogue for M ≥ 4.7 earthquakes. Ma et al. (1992) completed a complete

catalogue for M ≥ 6 earthquakes occurring in the SNSB and other two seismic belts as mentioned above during 1901 and 1990. After 1990, two M ≥ 6 destructive earthquakes were located in the SNSB, i.e., the 3 February 1996 M 6.6 Lijiang earthquake, Yunnan (YSB 1998) and the 12 May 2008 M 7.9 Wenchung earthquake (Cheng et al. 2009; Zhang et al. 2009). The two events caused severe damage in the respective surrounding areas. In addition to these two destructive earthquakes, several M ≥ 6 earthquakes occurred in the region after 1990. The earthquake data from those events were taken directly from the Earthquake Determination Report by US Geological Survey (USGS). The magnitude of the Wenchung earthquake was given as 8.0 by the China Earthquake Administration (CEA). Nevertheless, the magnitude value (M = 7.9) determined by USGS is taken in this study. Since Ma et al. (1992) corrected the earthquake magnitudes in their catalogue as the surface-wave magnitudes used by USGS. The magnitude scale is uniform for all data used in this study.

One hundred eighteen earthquakes with magnitudes from 6.0 - 8.5 are used in this study. Among them, 25 events had magnitudes ≥ 7. The occurrence dates, epicenters, and magnitudes of those earthquakes are listed in Table A1 in the appendix. The focal depths were not given by Ma et al. (1992) and thus not shown in Table A1. The pre-1967 earthquakes had higher uncertainties of epicentral location than the post-1967 events. However, at present it is difficult to accurately estimate the difference between the uncertainties of epicentral location in the two time periods. From Table A1, we can see five pairs of events, i.e., Events 3 and 4, Events 76 and 77, Events 90 and 91, Events 92 and 93, Events 95 and 96, and Events 104 and 105. For each pair, the two events happened close to each other in a short time span. Meanwhile, there was only a small difference between their magnitudes. The two events of a pair form an earthquake "doublet". An earthquake doublet is a pair of similarly sized earthquakes located relatively close together within short time duration. In addition, four sequent earthquakes, i.e., events 27, 28, 29, and 30, occurred in 1930 and 1931. The four events form an earthquake "quadruplet." An earthquake quadruplet includes four similarly sized earthquakes occurring relatively closely within short time duration. However, each doublet or quadruplet event is considered an individual one in this study. According to Bath's law (cf. Richter 1958), the magnitude of largest aftershock is, on the average, about 1.2 smaller than that of the mainshock. Hence, an M ≥ 8 earthquake will be followed by several M ≥ 7 aftershocks and an M ≥ 7 earthquake will be followed by several M ≥ 6 aftershocks. Hence, some events with magnitudes < 7 could be the aftershocks of relevant M ≥ 8 earthquakes. Figure 1 shows the plot of log(N) versus M and the straight line represents the least-squared equation: log(N) = (7.56 ± 0.19) - (0.90 ± 0.03)M, which is the frequency-magnitude law proposed by Gutenberg and Richter (1944).

Clearly, the data points are all around the straight line, thus suggesting data set completeness. Nevertheless, the data points for are slightly below the straight line. Hence, the fluctuation analysis will be conducted for three magnitude ranges with different lower-bound magnitudes, M_{low}, i.e., M_{low} = 6, 6.5, and 7.

The epicenters are displayed in Fig. 2. The epicentral distance between two events ranges from 0 - 2141.0 km
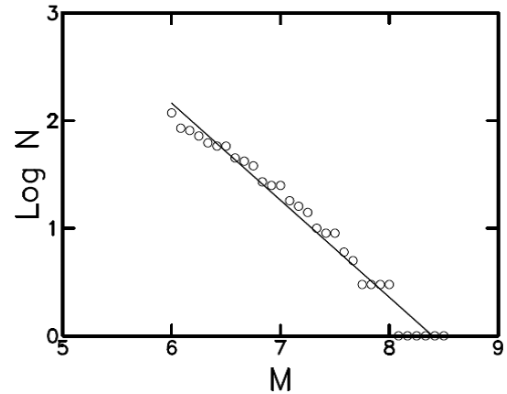

Fig. 1. Figure shows the plot of log(N) versus M, where N is the cumulative frequency, and the solid line is the least-squared equation: log(N) = (7.56 ± 0.19) - (0.90 ± 0.03)M.
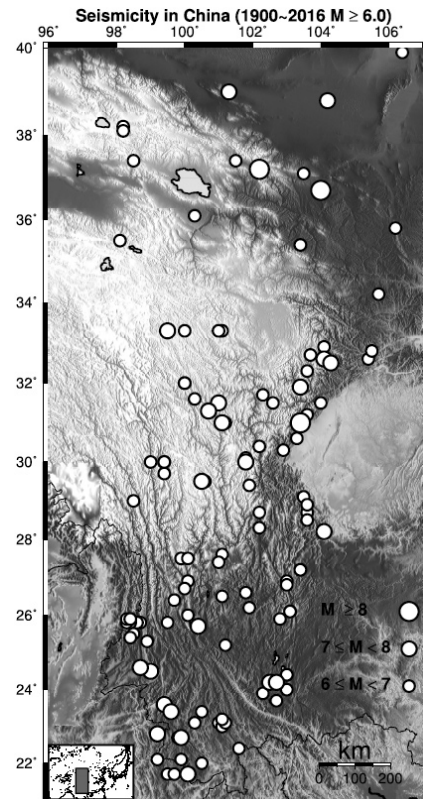

Fig. 2. Epicenters (shown by open circles) of M ≥ 6 earthquakes in the South-North Seismic Belt, Mainland China (longitudes from 98 - 107°E and latitudes from 21 - 41°N) during 1900 - 2016.

for M ≥ 6 events, from 0 - 1934.3 km for M ≥ 6.5 events, and from 22 - 1934.3 km for M ≥ 7 events. Figure 3 shows the earthquake sequences represented by magnitudes. The shortest inter-event time is smaller than 1 year for M ≥ 6, M ≥ 6.5, and M ≥ 7 events, and the shortest and longest inter-event times are, respectively, 0 and 12.27 years (with an average of 0.96 years) for M ≥ 6 events, 0 and 12.27 years (with an average of 1.93 years) for M ≥ 6.5 events, and 0 and 19.52 years (with an average of 4.15 years) for M ≥ 7 events. Since a few events occurred in a short time interval, the line segments representing them are close to one another and thus cannot be clearly separated.

3. METHODS

3.1 Multifractal Dimensions of Epicentral Distributions

A fractal set is defined as one in which the Hausdorff-Besicovitch dimension strictly exceeds the commonly-used topological dimension (Mandelbrot 1983). The fractal dimension is a characteristic fractal set index. However, it is not easy to apply the Hausdorff-Besicovitch's definition to estimate the fractal dimension in the real world. Several alternatives have been suggested to estimate the fractal dimension (cf. Takayasu 1990; Korvin 1992; Chen and Koyama 1995). Similarity dimension D_S is defined for an exact self-similar set as $D_S = \log L / \log N$, where L is the linear size and N is the number of similar daughters. Capacity dimension D_{CA} is defined as $D_{CA} = \log N(r) / \log(1/r)$, where $N(r)$ is the smallest number of coverings of a set with a size of r. Information dimension D_I is defined as $D_I = \Sigma p_i(r) \log[p_i(r)]/\log(r)$, where r is the distance between two points, based on the probabilistic distribution. Correlation dimension D_C is defined from the correlation integral C(r) in the following

relation: $C(r) \sim r^{D_c - d}$, where d = 2 is the spatial topological dimension and

$$C(r) = \lim[(\text{number of pairs whose distance is less than r})/N^2] \quad (1)$$

In general, $D_S = D_{CA} \geq D_I \geq D_C$ (Takayasu 1990), and D_C is the smallest value of the four fractal dimensions. The equality $D_S = D_{CA} = D_I = D_C$ holds only for a homogeneous fractal set. Most natural fractals are not completely self-similar and actually multifractal. For such fractals, we have $D_S = D_{CA} > D_I > D_C$. Hence, a single fractal dimension value is not enough to characterize the multifractal properties. Therefore, the fractal dimension has been extended to the generalized fractal dimension or multifractal dimension, D_q (Grassberger 1983; Hentschel and Procaccia 1983).

Generalized fractal dimension D_q is defined by the following expression:

$$D_q = (\lim\{\log[\Sigma_i p_i^q / \log(\delta)]\})/(q - 1) \quad (2)$$

where p_i is the probability that the events fall into a box with a length δ (Grassberger 1983; Hentschel and Procaccia 1983). The parameter q can take any real number in the range from $-\infty$ to ∞. D_q of large, positive q shows the fractal property of dense regions, where p_i is large, and D_q of large, negative q displays that of thin regions, where p_i is small. D_q for negative q can take a value larger than the spatial topological dimension d, thus calling D_q a dimension make no geometric sense for $D_q > d$ (Mandelbrot 1989). For q > 0, the largest D_q is D_0, and D_q decreases with increasing q. In
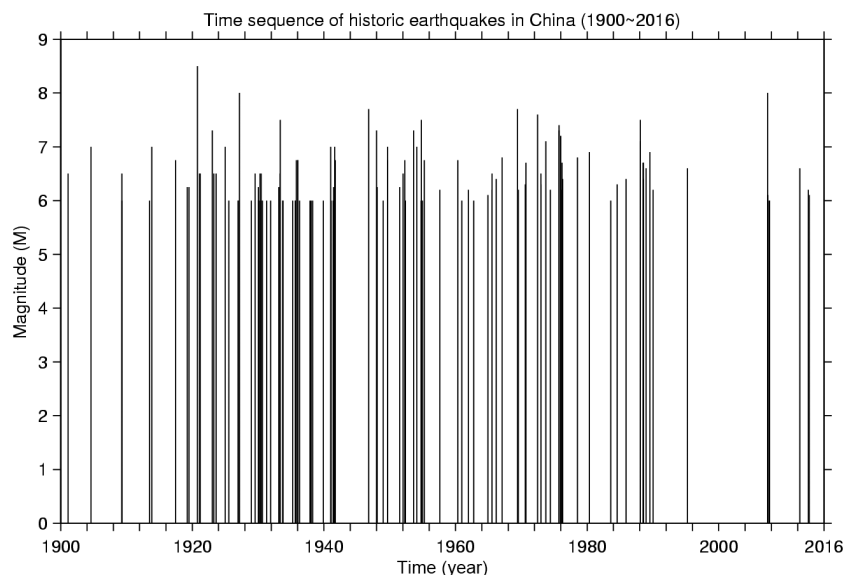

Fig. 3. Time sequences of M ≥ 6 earthquakes displayed in Fig. 1.

the cases of q = 0, 1, and 2, D_q relates to the capacity dimension D_{CA}, information dimension D_I, and correlation dimension D_C, respectively. The probability p_i can be estimated by the box-counting method from the observed data. However, the box-counting method requires a large number of data. An alternative correlation integral method was suggested by Kurths and Herzel (1987). A local density function $n_j(r)$ is defined by the following expression:

$$n_j(r) = \sum_k \Theta(r - |x_j - x_k|)/(N - 1) \qquad (3)$$

where the value of $\Theta(s)$ is 1 if $\delta r = r - |x_j - x_k| \geq 0$ and 0 if $\delta r < 0$. Conventionally, both r and $|x_j - x_k|$ were defined as the distance between two points (x_j, x_k).

A generalized correlation integral $C_q(r)$ for the epicentral distance, r, is defined by

$$C_q(r) = \left[\sum_j n_j^{q-1}(r)\right]^{1/(q-1)} \qquad (4)$$

$C_q(r)$ scales with r in the following form:

$$C_q(r) \sim r^{D_q} \qquad (5)$$

The D_q will be evaluated from the linear portion between $\log(r_1)$ and $\log(r_2)$ of the log-log plot of C_q versus r. In this study the D_q value at positive q is measured to establish the D_q-q relation for investigating multifractal behavior of epicentral distribution of earthquakes in use.

3.2 Multifractal Dimensions of Earthquake Time Sequences

In order to study the multifractal behavior of earthquake sequences, Wang and Lee (1995) replaced the two quantities r and $|r_i - r_k|$ by time interval t and inter-event time $|t_i - t_k|$ between two events, respectively. Wang (1996a) measured the generalized fractal dimensions at positive q for M ≥ 7 earthquake sequence in Taiwan. Wang and Lee (1995) and Wang (1996a) defined the local density function $n_j(t)$ to be:

$$n_j(t) = \sum_k \Theta(t - |t_j - t_k|)/(N - 1) \qquad (6)$$

where the $\Theta(s)$ value is 1 if $\delta t = t - |t_j - t_k| \geq 0$ and 0 if $\delta t < 0$. Hence, the generalized correlation integral $C_q(t)$ for the inter-event time, t, is

$$C_q(t) = \left[\sum_j n_j^{q-1}(t)\right]^{1/(q-1)} \qquad (7)$$

$C_q(t)$ scales with t in the following form:

$$C_q(t) \sim t^{D_q} \qquad (8)$$

The D_q will be evaluated from the linear portion between $\log(t_1)$ and $\log(t_2)$ of the log-log plot of C_q versus t. In this study the value of D_q at positive q is measured to establish the D_q-q relation for investigating multifractal behavior of earthquake sequences in use.

3.3 Morlet Wavelet Analysis for Earthquake Sequences

Assume that there is a time series, x_i, with an equal time spacing δt and n = 0 … N - 1 and $\psi(t)$ is a wavelet function of time t. To be "admissible" as a wavelet, $\psi(t)$ must have zero mean and be localized in both time and frequency space (Farge 1992). An example is the Morlet wavelet, named after Jean Morlet, was originally formulated by Goupillaud et al. (1984). The main function $\Psi(t)$ is composed of a harmonic wave, as a constant k_c subtracted from a plane wave, modulated by a Gaussian envelope. A detailed description about the technique can be found in Torrence and Compo (1998).

The wavelet is written as:

$$\psi(t) = A_c \pi^{-1/4} \exp(-t^2/2)[\exp(i\omega t) - k_c] \qquad (9)$$

where $A_c = [1 + \exp(-\omega^2) - 2\exp(-3\omega^2/4)]^{1/2}$ and $k_c = \exp(-\omega^2/2)$ and ω is the angular frequency (in Hz or s^{-1}). Pyrak-Nolte and Nolte (1995) reported $\omega = 2\pi/T_0$ where T_0 is the (characteristic) period of oscillations. In order to avoid some problems caused by small ω, $\omega > 5$ is usually taken into account. Farge (1992) took ω to be 6 to satisfy the admissibility condition. As $\omega = 6$, $T_0 = \sim 1$ s. As $\omega \gg 1$, Eq. (9) can be re-written as

$$\psi(t) = A_c \pi^{-1/4} \exp(-t^2/2)\exp(i\omega t) \qquad (10)$$

The continuous wavelet transform of a discrete sequence x_i is defined as the convolution of x_i with a scaled and translated version of $\psi(t)$:

$$W_n(s) = \sum_i x_i \psi^*[(i - n)\delta t/s] \quad (i = 0, ..., N - 1) \qquad (11)$$

where the (*) indicates the complex conjugate, δt is the time shift, and s is the wavelet scale. By varying the wavelet scale s and translating along the localized time index n, a picture can be constructed to show both the amplitude of any features versus the scale and how this amplitude varies with time. Although it is possible to calculate the wavelet transform using Eq. (11), it is considerably faster to do the calculations in Fourier space.

Because the wavelet function $\psi(t)$ is usually complex, the wavelet transform $W_n(s)$ is also complex. The transform can then be divided into the real part $R[W_n(s)]$ and the imaginary part $I[W_n(s)]$. Hence, the amplitude and phase are,

respectively, $|W_n(s)|$ and $\theta = \tan^{-1}\{R[W_n(s)]/I[W_n(s)]\}$. Finally, one can define the wavelet power spectrum as $|W_n(s)|^2$.

Let the discrete Fourier transform (DFT) of x_i be χ_k:

$$\chi_k = \sum_i x_i e^{-2\pi k n/N} \quad (i = 0, ..., N - 1) \qquad (12)$$

In the continuous limit, the Fourier transform of a function $\psi(t/s)$ is given by $F[\psi(s\omega)]$. By the convolution theorem, the wavelet transform is the inverse Fourier transform of the product:

$$W_n(s) = \sum_k \chi_k F[\psi * (s\omega_k)]\exp(i\omega_k n\delta t)$$
$$(k = 0, ..., N - 1) \qquad (13)$$

To ensure that the wavelet transforms at each scale s are directly comparable to each other and to the transforms of other time series, the wavelet function at each scale s is normalized to have unit energy:

$$F[\psi_o(s\omega_k)] = (2\pi s/\delta t)^{1/2} F[\psi(s\omega_k)] \qquad (14)$$

where $\int |F[\psi_o(\omega)]|^2 d\omega = 1$, that is, the function has been normalized to have unit energy.

Using the normalization in Eq. (14), and referring to Eq. (13), the expectation value for $|W_n(s)|^2$ is equal to N times the expectation value for $|\chi_k|^2$. For a white-noise time series, this expectation value is σ^2/N, where σ^2 is the variance. Thus, for a white-noise process, the expectation value for the wavelet transform is $|W_n(s)|^2 = \sigma^2$ at all n and s.

It is necessary to explain the significance levels of the calculated values. The null hypothesis is defined as follows: It is assumed that the time series has a mean power spectrum; when a peak in the wavelet power spectrum is significantly above this background spectrum, then it can be considered to be a true feature with a certain percentage of confidence. The 95% confidence level implies a test against a certain background level, while the 95% confidence interval refers to the range of confidence about a given value. The normalized Fourier power spectrum is given by $N|\chi_k|^2/2\sigma^2$, where N is the number of data points, χ_k is from Eq. (12), and σ^2 is the variance of the time series.

If x_n is a normally distributed random variable, both the real and imaginary parts of χ_k are normally distributed (Chatfield 1989). Since the square of a normally distributed variable is chi-square distributed with one degree of freedom (DOF), then $|\chi_k|^2$ is chi-square distributed with two DOFs, denoted by χ_2^2 (Jenkins and Watts 1968). To determine the 95% confidence level (significant at 5%), one multiplies the background spectrum by the 95th percentile value for χ_2^2 (Gilman et al. 1963). The 95% Fourier confidence spectrum will be displayed by a dashed curve below. Note that only at few periods, the power will be above the 95% line. The

dominant period is significant when its peak value is higher than the related 95% confidence level. The period associated with such a peak is taken to be the dominant period.

In order to meet the equal time interval requirement, we consider the number of events occurring in a year to represent the degree of earthquake occurrences. Hence, the dominant periods (with a unit of year) of time sequence for the number of yearly events are evaluated in the following.

4. RESULTS

4.1 Multifractal Dimensions of Epicentral Distributions

The generalized correlation integral functions, C_q, versus the epicentral distance, r, in kilometers between two earthquakes at q = 2, ..., 15 are calculated for three data sets with $M \geq 6$, $M \geq 6.5$, and $M \geq 7$ events in the study region. Since a few pairs of events have very similar epicenters, $C_q(r)$ at q = 0 and 1 cannot be evaluated. For simplification, only the log-log plots of $C_q(r)$ versus r at q = 2 (triangle), 6 (square), 10 (circle), and 14 (star) are plotted in Fig. 4a for $M \geq 6$ events, in Fig. 4b for $M \geq 6.5$ events, and in Fig. 4c for $M \geq 7$ events. It can be seen from Fig. 4 that when $r_l < r < r_u$, the data points are well distributed around a linear trend; while when $r < r_l$ or $r > r_u$, the data point pattern bends and departs from the linear trend. Bending or departure of the pattern indicates that the $\log C_q$ values for $r < r_l$ or $r > r_u$ are different from those estimated from the linear regression equation deduced from the data points with $r_l < r < r_u$. The r_l and r_2 values are, respectively, 120 km [$\log(r_l) = 2.08$] and 560 km [$\log(r_u) = 2.8$] for $M \geq 6$ events, 100 km [$\log(r_l) = 2.0$] and 560 km [$\log(r_u) = 2.8$] for $M \geq 6.5$ events, 65 km [$\log(r_l) = 1.8$] and 560 km [$\log(r_u) = 2.8$] for $M \geq 7$ events. The D_q value is evaluated from the data points in the linear range. The least-squared method is applied to infer a linear regression equation for the D_q estimation from the linear portion. The D_q values are between 1.618 and 1.426, with standard deviations from 0.001 - 0.003, for $M \geq 6$ events, between 1.562 and 1.108, with standard deviations from 0.001 - 0.003, for $M \geq 6.5$ events, and between 1.365 and 0.841, with standard deviations from 0.001 - 0.003, for $M \geq 7$ events. The D_q-q relation is displayed in Fig. 5: solid circles for $M \geq 6$ events, solid squares for $M \geq 6.5$ events, and solid triangles for $M \geq 7$ events. The D_q error for each q is less than 0.003 for $M \geq 6$, $M \geq 6.5$, and $M \geq 7$ events.

4.2 Multifractal Dimensions of Time Sequences

The generalized correlation integral functions, C_q, versus inter-event time, t, in years between two earthquakes at q = 2, ..., 15 are calculated for two data sets with $M \geq 6$ and $M \geq 7$ earthquakes in the study region. Since a few pairs of events have very similar occurrence times, the $C_q(r)$ values at q = 0 and 1 cannot be evaluated. For simplification, only the log-log plots of $C_q(t)$ versus t at q = 2 (triangle), 6

(square), 10 (circle), and 14 (star) are plotted in Fig. 6a for M ≥ 6 events, in Fig. 6b for M ≥ 6.5 events, and in Fig. 6c for M ≥ 7 events. It can be seen from Fig. 6a that when $t_l < t < t_u$, where $t_l = 5$ years [$\log(t_l) = 0.7$] and $t_u = 50.1$ years [$\log(t_u) = 1.8$], the data points are well distributed around a linear trend; while when $t < t_l$ or $t > t_u$, the data point pattern bends and departs from the linear trend. The bending pattern indicates that the $\log C_q$ value for $t > t_u$ is less than that estimated from the linear regression equation deduced from the data points with $t_l < t < t_u$. From Fig. 6b for M ≥ 6.5 events, we can see that when $t_l < t < t_u$, where t_l and t_u are, respectively, 5 years [$\log(t_l) = 0.7$] and 50.1 years [$\log(t_u) = 1.8$], the data points are well distributed around a linear trend; while when $t < t_l$ or $t > t_u$, the pattern of data points bends and departs from the linear trend. From Fig. 6c for M ≥ 7 events, we can see that when $t_l < t < t_u$, where t_l and t_u are, respectively, 16 years [$\log(t_l) = 1.2$] and 63 years [$\log(t_u) = 1.8$], the data points are well distributed around a linear trend. When $t < t_l$ or $t > t_u$, the data point pattern bends and departs from the linear trend.

The least-squared method is applied to infer a linear regression equation for the D_q estimation from the linear portion. The D_q values are between 0.830 and 0.703, with a standard deviation of 0.001. For M ≥ 6 events between 0.835 and 0.820, with standard deviation of 0.001, for M ≥ 6.5 events, and between 0.786 and 0.685, with standard deviations from 0.002 - 0.004, for M ≥ 7 events. The D_q-q relation is displayed in Fig. 7: solid circles for M ≥ 6 events, solid squares for M ≥ 6.5 events, and solid triangles for M ≥ 7 events. The D_q error for each q is less than 0.001 for M ≥ 6 and M ≥ 6.5 events and less than 0.004 for M ≥ 7 events.

4.3 Morlet Wavelet Analysis for Earthquake Sequences

The Morlet wavelet analysis results are displayed in Figs. 8 - 10: Fig. 8 for M ≥ 6 events, Fig. 9 for M ≥ 6.5

events, and Fig. 10 for M ≥ 7 events. Each figure consists of three panels: (a) for the time sequence of the number of yearly events; (b) for the wavelet power spectrum; and (c) for the global wavelet spectrum. In panel (b) the logarithmic wavelet power spectrum values for different periods (in year) at a certain time span are displayed using distinct colors (from dark red to dark blue). The thick contour is the 95% confidence level using a white-noise background spectrum. The black net region is the cone of influence, where zero padding has reduced the variance. The wavelet power spectrum values inside the net have high uncertainties and thus cannot be taken into account. In each panel (b), the local maximums and local minimums are colored, respectively, by dark red and dark blue. The period related to the local maximum is the local dominant period in a time span. In order to examine the dominant local maximum and related dominant period it is necessary to calculate the average wavelet power spectra from panel (b) over time at a certain period. This average is named the global wavelet spectrum. The results are demonstrated in panel (c), where the solid line represents the global wavelet spectrum and the dashed line denotes the 95% confidence level using a white-noise background spectrum.

Figure 8a shows the time sequence for the yearly number of events for M ≥ 6 earthquakes. Figure 8b shows the wavelet transform power spectrum for the yearly events. The local maximums at several periods in different time spans can be seen. Figure 8c shows that the global wavelet spectrum value obviously increases at the large period around 32 years. Meanwhile, except at a period of 2.92 years the solid line is to the left of the 95% confidence level dashed line.

Figure 9a shows the time sequence of the number of yearly events for M ≥ 6.5 earthquakes. Essentially, there was only one spike in 1975. The wavelet power spectra of the time sequence is quite abnormal, as shown in Fig. 9b.

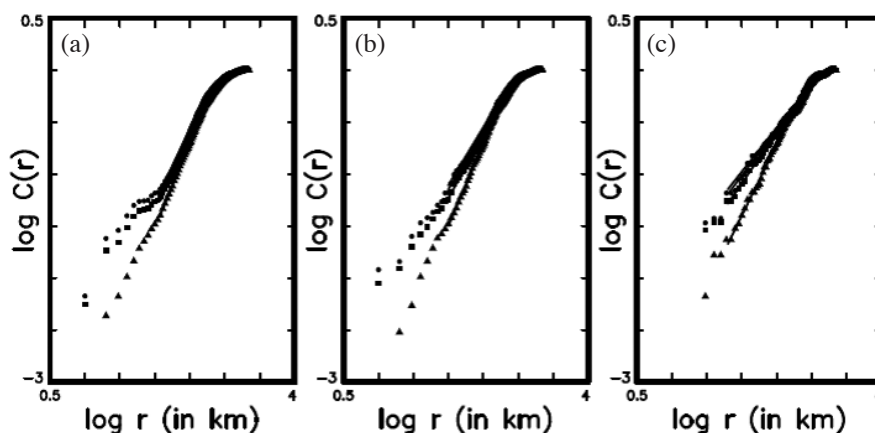

Fig. 4. The log-log plots of $C_q(r)$ versus r at q = 2 (triangle), 6 (square), 10 (circle), and 14 (star) for the epicentral distributions in the study region: (a) for M ≥ 6 events; (b) for M ≥ 6.5; and (c) for M ≥ 7 events. The solid lines represent the regression lines inferred from the data points with $\log(r_1) \le \log(r) \le \log(r_2)$, where r_1 and r_2 are explained in the text.

Fig. 5. The plot of D_q versus q from Fig. 4: solid circles for M ≥ 6 events, solid squares for M ≥ 6.5 events, solid triangles for M ≥ 7 events, and open circles for the data from Wang and Shen (1999).
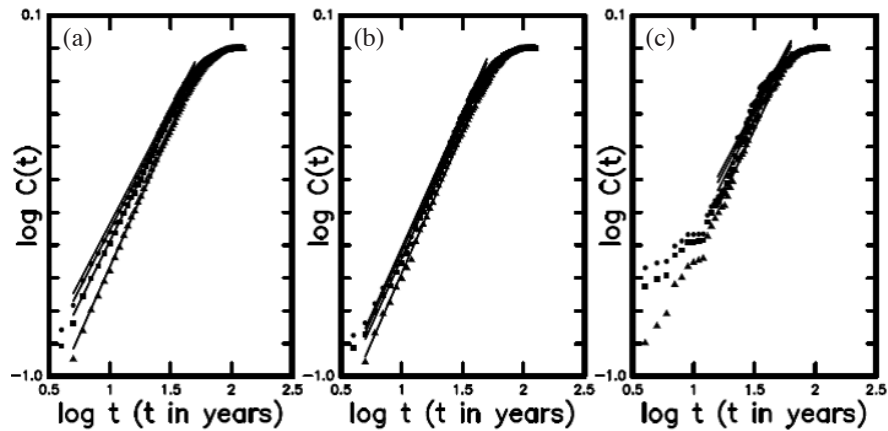
Fig. 6. The log-log plots of $C_q(t)$ versus t at q = 2 (triangle), 6 (square), 10 (circle), and 14 (star) for the time sequences in the study region: (a) for M ≥ 6 events; (b) for M ≥ 6.5; and (c) for M ≥ 7 events. The solid lines represent the regression lines inferred from the data points with $\log(t_1) \le \log(t) \le \log(t_2)$, where t_1 and t_2 are explained in the text.
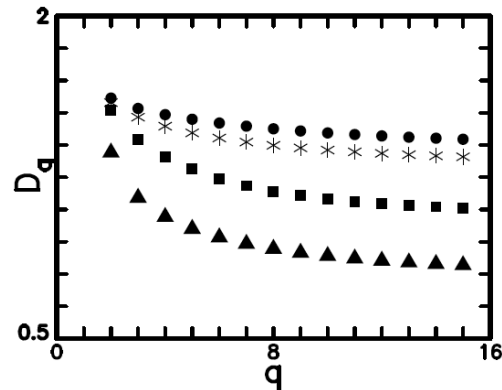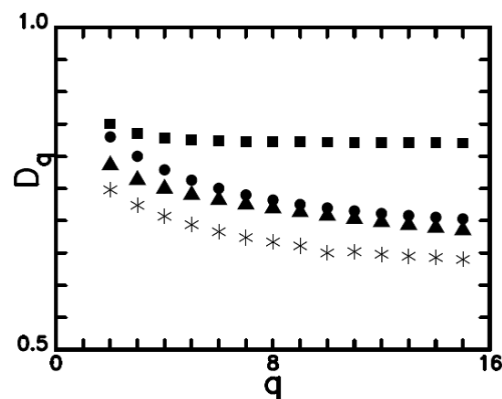

Fig. 7. The plot of D_q versus q from Fig. 6: solid circles for M ≥ 6 events, solid squares for M ≥ 6.5 events, solid triangles for M ≥ 7 events, and open circles for the data from Wang and Lee (1995).

Fig. 8. The figure shows (a) the time sequence for the number of yearly events with M ≥ 6; (b) the wavelet power spectrum; and (c) the average or the global wavelet spectrum of (b) over all longitudes. In (b) the thick contour is the 95% confidence level, using a white-noise background spectrum. The black net is described in the text. The dashed line is the 95% confidence level for the global wavelet spectrum, using a white-noise background spectrum.

Fig. 9. The figure shows (a) the time sequence for the number of yearly events with M ≥ 6.5; (b) the wavelet power spectrum; and (c) the average or the global wavelet spectrum of (b) over all longitudes. In (b) the thick contour is the 95% confidence level, using a white-noise background spectrum. The black net is described in the text. The dashed line is the 95% confidence level for the global wavelet spectrum, using a white-noise background spectrum.

Fig. 10. The figure shows (a) the time sequence for the number of yearly events with M ≥ 7; (b) the wavelet power spectrum; and (c) the average or the global wavelet spectrum of (b) over all longitudes. In (b) the thick contour is the 95% confidence level, using a white-noise background spectrum. The black net is described in the text. The dashed line is the 95% confidence level for the global wavelet spectrum, using a white-noise background spectrum.

Although there are several peaks in Fig. 9c, their spectral values are lower than the 95% confidence level and the solid line is to the left of the dashed line. Hence, there is no dominant period for the M ≥ 6.5 earthquake sequence.
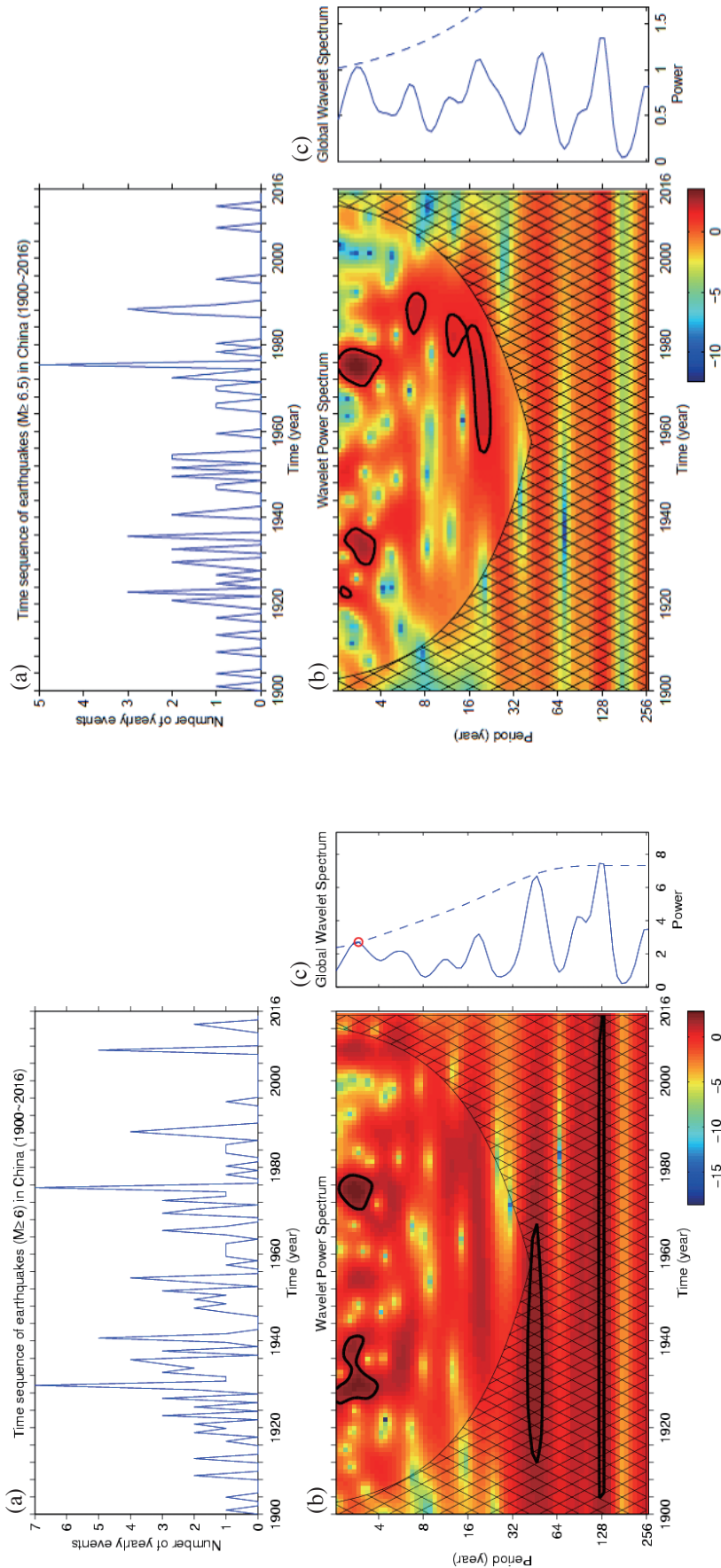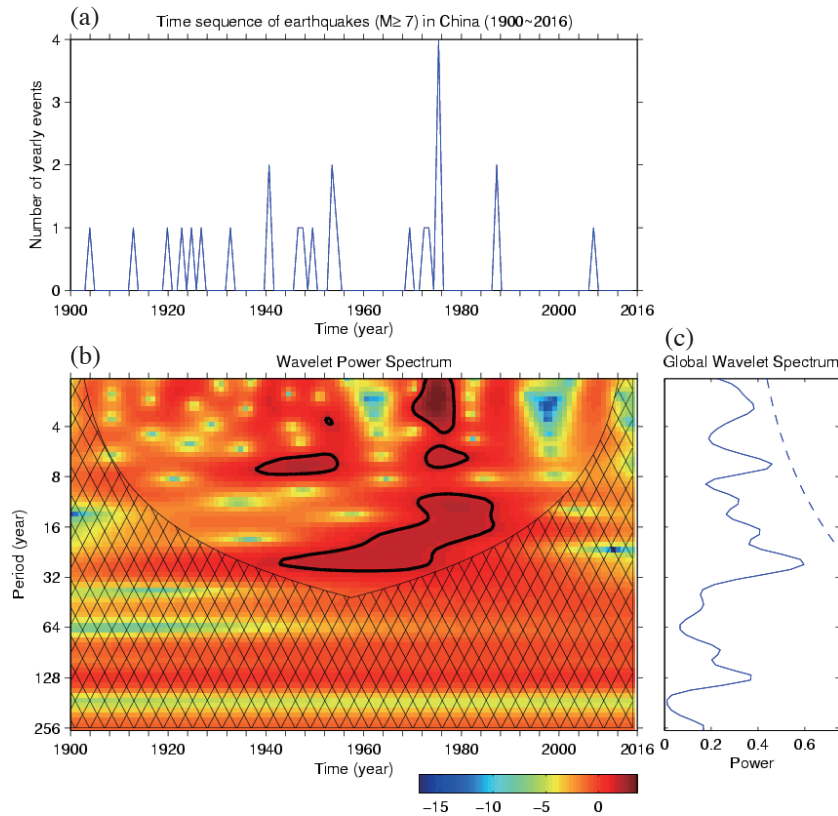
Figure 10a shows the time sequence of the number of yearly events for M ≥ 7 earthquakes. Essentially, there was only one spike in 1975. The wavelet power spectra of the time sequence is quite abnormal, as shown in Fig. 10b. Although there are several peaks in Fig. 10c, their spectral values are lower than the 95% confidence level and the solid line is to the left of the dashed line. Hence, there is no dominant period for the M ≥ 7 earthquake sequence.

5. DISCUSSION

From Fig. 2 we can see that the epicentral spatial distribution is not uniform for both M ≥ 6 and M ≥ 7 events in the whole area. It seems that the number of events per unit area is higher in the southern area than in the northern. Figure 3 shows that the temporal variation in events is not uniform in the whole time period. The frequency of events is relatively low before 1920 and after 1986.

Figure 4 reveals that the log-log plots of C_q versus r

show a linear portion when $r_l < r < r_u$. The pattern bends when $\log(r) < \log(r_l)$ and bends as well as becomes flat when $\log(r) > \log(r_u)$. The value of $r_1 = 120$ km for M ≥ 6 events is longer than $r_1 = 100$ km for M ≥ 6.5 events and $r_1 = 64$ km for M ≥ 7 events. The value of $r_2 = 560$ km is almost the same for M ≥ 6, M ≥ 6.5, and M ≥ 7 events. This means that the range of epicentral distances exhibiting multifractal properties is narrower for M ≥ 6 events than for M ≥ 6.5 and M ≥ 7 events. Clearly, the number of data points with $r < r_1$ is larger than that with $r > r_1$ for M ≥ 6 events. This might be because some M ≥ 6 events, especially for M < 6.5 events, are aftershocks of M ≥ 7 earthquakes. Meanwhile, the data points with $\log(r) < \log(r_l)$ for M ≥ 6 events are more dispersive than those for M ≥ 6.5 and M ≥ 7 events. The D_q values from q = 2 to q = 15 are between 1.618 and 1.426 for M ≥ 6 events, between 1.562 and 1.108 for M ≥ 6.5 events, and between 0.841 for M ≥ 7 events. Clearly, the D_q values are smaller for M ≥ 7 events than for M ≥ 6 events. This means the epicentral distribution is sparser for M ≥ 7 events than for M ≥ 6.5 and M ≥ 6 events. This is reasonable, because the density of events is higher for M ≥ 6 and M ≥ 6.5 events than for M ≥ 7 events as displayed in Fig. 2.

Figure 5 shows that the D_q-q relations of epicenter for

the three magnitude ranges. Obviously, D_q decreases with increasing q. The difference in the D_q values for the three magnitude ranges increase slightly with q. From the epicentral distributions and numbers of events, the spatial distribution of M ≥ 6 events is denser than those of M ≥ 6.5 and M ≥ 7 events. Hence, based on fractal geometry D_q at positive q should be larger for M ≥ 6 events than those of M ≥ 6.5 and M ≥ 7 events. The D_q values for the three magnitude ranges are smaller than the topological dimension d = 2 of two-dimensional space. This indicates that the spatial distributions of those earthquakes are sparse. For the purpose of comparison, the D_q-q relation for M ≥ 6 events occurred from 1900 to 1990 in the study region obtained by Wang and Shen (1999) is also plotted in Fig. 5 using stars. Their data are the same as those from 1900 - 1990 used in this study. Their D_q-q relation is close to that in this study; while their D_q values are slightly smaller than those in this study. The addition of events after 1990 only slightly increases the D_q values, in other words, only slight increases the density of spatial distribution of earthquakes.

Figures 6 displays that the log-log plot of $C_q(t)$ versus t show a linear distribution when $\log(t_l) \leq \log(t) \leq \log(t_u)$, where t_l and t_u are, respectively, 5 and 50.1 years for M ≥ 6 events, 5 and 50.1 years for M ≥ 6.5 events, and 16 years and 63.1 years for M ≥ 7 event, thus suggesting that the earthquake sequences in the study region are multifractal. For M ≥ 6 events, the pattern bends and becomes flat when $\log(t) > \log(t_u)$; while for M ≥ 6.5 and M ≥ 7 event, the pattern bends when $\log(t) < \log(t_l)$ and bends as well as becomes flat when $\log(t) > \log(t_u)$. The D_q values from q = 2 to q = 15 are between 0.830 and 0.703 for M ≥ 6 events, between 0.850 and 0.820 for M ≥ 6.5 events, and between 0.786 and 0.685 for M ≥ 7 events. This means that the range of inter-event times for the existence of multifractal properties is wider for M ≥ 6.5 events than for both M ≥ 6 and M ≥ 7 events. Although the D_q value for M ≥ 6, M ≥ 6.5, and M ≥ 7 events are smaller than the topological dimension d = 1 of one-dimensional time series, they do not depart from d = 1 too much. This indicates that within the time period in consideration, the earthquake sequences are only slightly sparse.

Figure 7 shows that the D_q-q relations of inter-event times for the three magnitude ranges. Obviously, D_q decreases with increasing q. Unlike the epicentral distributions, the D_q values are larger for M ≥ 6.5 events than both M ≥ 6 and M ≥ 7 events. Comparing Figs. 7a with b exhibits that the log(t) ranges for the D_q estimates are almost the same for both M ≥ 6 and M ≥ 6.5 events and the log[C(t)] values at small t are higher for the former than for the latter. This leads to larger D_q for M ≥ 6 events than for M ≥ 6.5 events. On the other hand, D_q is evaluated from a narrower range of log(t) for M ≥ 7 events. The difference in the D_q values between M ≥ 6.5 events and M ≥ 6 events as well as between M ≥ 6.5 events and M ≥ 7 events increases with q. The difference in the D_q values between M ≥ 6 events and M ≥ 7 events

slightly decreases with increasing q. Although the temporal variations and numbers of events for M ≥ 6 and M ≥ 7 are different and the temporal variation of M ≥ 6 events is denser than that of M ≥ 7 events, the difference in D_q between the two magnitude ranges is small. For comparison, the D_q-q relation for M ≥ 6 events occurred from 1900 - 1990 in the study region obtained by Wang and Lee (1995) are also plotted in Fig. 7 using the solid square. Their data are the same as those from 1900 to 1990 used in this study. Their D_q-q relation is nearly parallel to that of this study; while their D_q values are smaller than those in this study. The addition of events after 1990 only slightly increases the D_q values.

For the New Hebrides seismicity between mid-1978 and mid-1984, Smalley et al. (1987) found that the fractal dimension varies from 0.126 - 0.255 and the earthquake occurrences deviate significantly from random or Poisson behavior. Kagan and Jackson (1991) stated that for 1-D processes, if the correlation dimension equals 1 over all time periods from zero to infinity, the process is Poissonian. For global seismicity, they found that long-term, weak clustering characterizes all mainshocks and is governed by a power-law temporal distribution. They also mentioned that the fractal dimension of the set of earthquakes on the time axis is of the order of 0.8 - 0.9, thus, mainshock occurrence is closer to a stationary Poisson process. Gardner and Knopoff (1974) stated that the M ≥ 2.8 mainshock time series in Southern California, USA, during 1932 - 1971 is Poissonian. The fractal dimension used by these authors is the correlation dimension and equivalent to D_2 in this study. Their results suggest that the time sequence for earthquakes with a higher D_2 has a stronger Poissonian process component. The D_2 value is 0.830 for M ≥ 6 events, 0.835 for M ≥ 6.5 events, and 0.785 for M ≥ 7 events. Hence, in comparison with the global seismicity, the Poissonian process component in the earthquake sequences of the seismic belt in this study is strong. For M ≥ 6 earthquakes occurring in the 1900 - 1990 period in the study region, Wang and Kuo (1995) found that both the exponential function and gamma function can describe the distributions and the former is more appropriate than the latter. This indicates that the earthquake sequence in the study region has a significant Poissonian process component. Wang (2013) also found that the earthquake sequence in the study region shows a weak memory effect and thus has a strong Poissonian process component. Moreover, the M ≥ 7 earthquake sequence is more Poissonian than the M ≥ 6 and M ≥ 6.5 ones. This is also consistent with the conclusion made by Wang (2013).

Figure 8a shows the time sequence for the number of yearly events for M ≥ 6 earthquakes. There were several large spikes in the time period before 1990. This means that seismicity was higher before 1990 than after 1990. Figure 8c shows that for the M ≥ 6 earthquake sequence, peaks exist at several periods in the solid line. However, only the global wavelet spectral value at 2.92 years is slightly to the right

of the dashed line representing the 95% confidence level. Hence, there is only one dominant period of 2.92 years for the $M \geq 6$ earthquake sequence. This dominant period is about three times longer than the average inter-event time of 0.96 years.

Figure 9a shows the time sequence for the number of yearly events for $M \geq 6.5$ earthquakes. There was only one spike in 1975. Figure 9c shows that for $M \geq 6.5$ earthquakes there are peaks in the solid line at several periods. However, their global wavelet spectral values are all to the left of the dashed line representing the 95% confidence level. Hence, there is no dominant period for the $M \geq 6.5$ earthquake sequence. As mentioned previously, the number of $M \geq 6.5$ earthquakes is relatively small and thus their wavelet power spectrum (Fig. 9b) and the global wavelet spectrum (Fig. 9c) are not normal. Hence, $M \geq 6.5$ earthquakes in the study region are not dominant.

Figure 10a shows the time sequence for the number of yearly events for $M \geq 7$ earthquakes. There was only one spike in 1975. Figure 10c shows that for $M \geq 7$ earthquakes there are peaks in the solid line at several periods. However, their global wavelet spectral values are all to the left of the dashed line representing the 95% confidence level. Hence, there is no dominant period for the $M \geq 7$ earthquake sequence. As mentioned previously, the number of $M \geq 7$ earthquakes is relatively small and thus their wavelet power spectrum (Fig. 10b) and the global wavelet spectrum (Fig. 10c) are not normal. Hence, $M \geq 7$ earthquakes in the study region are not dominant.

6. CONCLUSIONS

The generalized fractal dimensions are measured for $M \geq 6$ earthquakes in the South-North Seismic Belt, Mainland China (longitudes from 98 - 107°E and latitudes from 21 - 41°N) during 1900 - 2015 based on the spatial distribution (using the epicentral distances between two events, r) and the earthquake sequence (using the inter-event time between two events, t). The epicentral distance between two events ranges from 0 - 2141.0 km for $M \geq 6$ events, from 0 - 2141.0 km for $M \geq 6.5$ events, and from 0 - 1934.0 km for $M \geq 7$ events. Multifractal measures are made from the log-log plot of $C_q(r)$ versus r and that of $C_q(t)$ versus t. The plots show a linear distribution of data points when $\log(r_l) \leq \log(r) \leq \log(r_u)$ and roll-over when $\log(r) > \log(r_u)$. The r_l and r_u values are, respectively, 120 and 560 km for $M \geq 6$ events, 100 and 560 km for $M \geq 6.5$ events, and 65 and 560 km for $M \geq 7$ events. The D_q value, which is the slope of the linear portion, is between 1.618 and 1.426 for $M \geq 6$ events, between 1.562 and 1.108 for $M \geq 6.5$ events, and between 1.365 and 0.841 for $M \geq 7$ events. For the three magnitude ranges, D_q monotonically decreases with increasing q, thus indicating that the epicentral distributions show multifractal behavior. The D_q values are smaller than the topological di-

mension d = 2 for the two-dimensional surface.

The log-log plot of $C_q(t)$ versus t show a linear distribution when $\log(t_l) \leq \log(t) \leq \log(t_u)$, where t_l and t_u are, respectively, 5 and 50.1 years for $M \geq 6$ events, 5 and 50.1 years for $M \geq 6$ events, 16 and 63.1 years for $M \geq 7$ event, thus suggesting that the earthquake time sequences in the study region are multifractal. The D_q values are between 0.830 and 0.703 for $M \geq 6$ events, between 0.835 and 0.820 for $M \geq 6.5$ events, and between 0.786 and 0.685 for $M \geq 7$ events. For the three magnitude ranges, D_q monotonically decreases with increasing q, thus indicating that the earthquake sequences show multifractal behavior. The D_q values are all smaller than the topological dimension d = 1 of the one-dimensional time series. The $M \geq 7$ earthquake sequence is more Poissonian than the $M \geq 6$ and $M \geq 6.5$ ones.

The Morlet wavelet technique is applied to analyze the dominant temporal variation periods in numbers of yearly events for the three magnitude ranges, i.e., $M \geq 6$, $M \geq 6.5$, and $M \geq 7$. In the time domain the average inter-event time is 0.96 years for $M \geq 6$ events, 1.93 years for $M \geq 6.5$ events, and 4.15 for $M \geq 7$ events. The resultant dominant period is 2.92 years, which is about three times of 0.96 years, for $M \geq 6$ events and cannot be evaluated for $M \geq 6.5$ and $M \geq 7$ events.

REFERENCES

Aki, K., 1982: A probabilistic synthesis of precursor phenomena. In: Simpson, D. W. and P. G. Richards (Eds.), Earthquake Prediction, AGU, Washington D.C., USA, 556-574, doi: 10.1029/ME004p0566. [Link]

Aochi, H. and S. Ide, 2004: Numerical study on multi-scaling earthquake rupture. *Geophys. Res. Lett.*, **31**, L02606, doi: 10.1029/2003GL018708. [Link]

ASIG (Academia Sinica, Institute of Geophysics), 1975: Summary of large earthquakes in China from 780 B.C. to 1973 A.D. with magnitudes≥6, Academia Sinica, Peking, 31 pp. (in Chinese)

Aviles, C. A., C. H. Scholz, and J. Boatwright, 1987: Fractal analysis applied to characteristic segments of the San Andreas fault. *J. Geophys. Res.*, **92**, 331-344, doi: 10.1029/jb092ib01p00331. [Link]

Avouac, J. P. and P. Tapponnier, 1993: Kinematic model of active deformation in Central Asia. *Geophys. Res. Lett.*, **20**, 895-898, doi: 10.1029/93gl00128. [Link]

Candela, T., F. Renard, Y. Klinger, K. Mair, J. Schmittbuhl, and E. E. Brodsky, 2012: Roughness of fault surfaces over nine decades of length scales. *J. Geophys. Res.*, **117**, B08409, doi: 10.1029/2011JB009041. [Link]

Chatfield, C., 1989: The Analysis of Time Series: An Introduction, 4th edition, Chapman and Hall, 241 pp.

Chen, K. C., J. H. Wang, K. H. Kim, W. G. Huang, K. H. Chang, J. C. Wang, and P. L. Leu, 2015: Morlet wavelet analysis of $M_L \geq 3$ earthquakes in the Taipei Metropolitan Area. *Terr. Atmos. Ocean. Sci.*, **26**, 83-94, doi: 10.3319/TAO.2014.09.09.01(T). [Link]

Chen, Y. and J. Koyama, 1995: Fractal geometry and geoscience. In: Koyama, J. and D. Feng (Eds.), Advance in Mathematical Seismology, Seismological Press, Beijing, 1-29.

Chen, Y. T., Z. L. Wang, and B. Q. Wang, 1994: Seismological studies of earthquake prediction in China: A review. In: Dragoni, M. and E. Boschi (Eds.), Earthquake Prediction, 71-109.

Cheng, W., Z. Zhang, and X. Ruan, 2009: Spatio-temporal variation and focal mechanism of the Wenchuan $M_s8.0$ earthquake sequence. *Earthq. Sci.*, **22**, 109-117, doi: 10.1007/s11589-009-0109-z. [Link]

Combes, J. M., A. Grossman, and P. Tchamitchian, 1989: Wavelets: Time-Frequency Methods and Phase Space. Springer-Verlag, Berlin, 331 pp, doi: 10.1007/978-3-642-97177-8. [Link]

Daubechies, I., 1990: The wavelet transform, time-frequency localization and signal analysis. *IEEE Trans. Inform. Theor.*, **36**, 961-1005, doi: 10.1109/18.57199. [Link]

Farge, M., 1992: Wavelet transforms and their applications to turbulence. *Annu. Rev. Fluid Mech.*, **24**, 395-457, doi: 10.1146/annurev.fluid.24.1.395. [Link]

Gardner, J. K. and L. Knopoff, 1974: Is the sequence of earthquakes in southern California, with aftershocks removed, Poissonian? *Bull. Seismol. Soc. Am.*, **64**, 1363-1367.

Gilman, D. L., F. J. Fuglister, and J. M. Mitchell Jr., 1963: On the power spectrum of "red noise". *J. Atmos. Sci.*, **20**, 182-184, doi: 10.1175/1520-0469(1963)020<0182:OTPSON>2.0.CO;2. [Link]

Goupillaud, P., A. Grossman, and J. Morlet, 1984: Cycle-octave and related transforms in seismic signal analysis. *Geoexploration*, **23**, 85-102, doi: 10.1016/0016-7142(84)90025-5. [Link]

Grassberger, P., 1983: Generalized dimensions of strange attractors. *Phys. Lett.*, **97**, 227-230, doi: 10.1016/0375-9601(83)90753-3. [Link]

Gutenberg, B. and C. F. Richter, 1944: Frequency of earthquakes in California. *Bull. Seismol. Soc. Am.*, **34**, 185-188.

Hentschel, H. G. E. and I. Procaccia, 1983: The infinite number of generalized dimensions of fractals and strange

attractors. *Phys. Nonlinear Phenom.*, **8**, 435-444, doi: 10.1016/0167-2789(83)90235-x. [Link]

Hirabayashi, T., K. Ito, and T. Yoshii, 1992: Multifractal analysis of earthquakes. *Pure Appl. Geophys.*, **138**, 591-610, doi: 10.1007/bf00876340. [Link]

Hirata, T., 1989: A correlation between the *b* value and the fractal dimension of earthquakes. *J. Geophys. Res.*, **94**, 7507-7514, doi: 10.1029/jb094ib06p07507. [Link]

Hsieh, Y. S., D. L. Cheng, and S. J. Yu, 1989: Catalogue of Chinese Earthquakes (M4.7) from 1900 to 1980 with Uniform Magnitudes, Seismology Press, Beijing, 137 pp. (in Chinese)

Huan, W. and Z. Shi, 1987: Great earthquakes of M≥8 in the mainland of China and their evolution. *Tectonophysics*, **138**, 55-68, doi: 10.1016/0040-1951(87)90065-5. [Link]

Ide, S. and H. Aochi, 2005: Earthquakes as multiscale dynamic ruptures with heterogeneous fracture surface energy. *J. Geophys. Res.*, **110**, B11303, doi: 10.1029/2004JB003591. [Link]

Ide, S. and H. Aochi, 2014: Modeling earthquakes using fractal circular patch models with lessons from the 2011 Tohoku-Oki earthquake. *J. Disast. Res.*, **9**, 264-271, doi: 10.20965/jdr.2014.p0264. [Link]

Jenkins, G. M. and D. G. Watts, 1968: Spectral Analysis and Its Applications, Holden-Day, 525 pp.

Kagan, Y. Y., 2007: Earthquake spatial distribution: The correlation dimension. *Geophys. J. Int.*, **168**, 1175-1194, doi: 10.1111/j.1365-246X.2006.03251.x. [Link]

Kagan, Y. Y. and D. D. Jackson, 1991: Long-term earthquake clustering. *Geophys. J. Int.*, **104**, 117-134, doi: 10.1111/j.1365-246x.1991.tb02498.x. [Link]

Korvin, G., 1992: Fractal models in the Earth Sciences. Elsevier, Amsterdam, London, New York, Tokyo, 396 pp.

Koyama, J., S. X. Zang, and T. Ouchi, 1995: Mathematical modeling and stochastic scaling of complex earthquake activity. In: Koyama, J. and D. Feng (Eds.), Advance in Mathematical Seismology, Seismological Press, Beijing, 165-180.

Ku, K. S., 1983a: Chinese Earthquake Catalogue (1831 B.C. to 1969 A.D.), Science Press, Beijing, 894 pp. (in Chinese)

Ku, K. S., 1983b: Chinese Earthquake Catalogue (1970 to 1979), Science Press, Beijing, 334 pp. (in Chinese)

Kurths, J. and H. Herzel, 1987: An attractor in a solar time series. *Phys. Nonlinear Phenom.*, **25**, 165-172, doi: 10.1016/0167-2789(87)90099-6. [Link]

Lee, H. K. and H. P. Schwarcz, 1995: Fractal clustering of fault activity in California. *Geology*, **23**, 377-380, doi: 10.1130/0091-7613(1995)023<0377:FCOFAI>2.3.CO;2. [Link]

Lee, W. H. K., F. T. Wu, and S. C. Wang, 1978. A catalog of instrumentally determined earthquakes in China

(magnitude≥6) compiled from various sources. *Bull. Seismol. Soc. Am.*, **68**, 383-398.

Lee, Y. T., K. F. Ma, and Y. T. Yen, 2016: Heterogeneous slip distribution self-similarity on a fault surface. *Terr. Atmos. Ocean. Sci.*, **27**, 181-193, doi: 10.3319/TAO.2015.11.05.01(T). [Link]

Li, S., 1960: Chinese earthquake Catalogue. Science Press. (in Chinese)

Ma, Z., X. Li, and J. Jin, 1992: The law interpretation and prediction of earthquake migration-Earthquake Migration of four seismic belts in China Mainland. *Seismol. Geol.*, **14**, 129-139. (in Chinese)

Main, I., 1996: Statistical physics, seismogenesis, and seismic hazard. *Rev. Geophys.*, **34**, 433-462, doi: 10.1029/96rg02808. [Link]

Mandelbrot, B. B., 1983: The Fractal Geometry of Nature. W.H. Freeman, New York, 468 pp.

Mandelbrot, B. B., 1989: Multifractal measures, especially for the geophysicist. *Pure Appl. Geophys.*, **131**, 5-42, doi: 10.1007/bf00874478. [Link]

Manighetti, I., M. Campillo, C. Sammis, P. M. Mai, and G. King, 2005: Evidence for self-similar, triangular slip distributions on earthquakes: Implications for earthquake and fault mechanics. *J. Geophys. Res.*, **110**, B05302, doi: 10.1029/2004JB003174. [Link]

Michas, G., P. Sammonds, and F. Vallianatos, 2014: Dynamic multifractality in earthquake time series: Insights from the Corinth rift, Greece. *Pure Appl. Geophys.*, **172**, 1909-1921, doi: 10.1007/s00024-014-0875-y. [Link]

Molnar, P. and P. Tapponnier, 1975: Cenozoic tectonics of Asia: Effects of a continental collision: Features of recent continental tectonics in Asia can be interpreted as results of the India-Eurasia collision. *Science*, **189**, 419-426, doi: 10.1126/science.189.4201.419. [Link]

Morlet, J., G. Arens, E. Fourgeau, and D. Giard, 1982: Wave propagation and sampling theory - Part II: Sampling theory and complex waves. *Geophysics*, **47**, 222-236, doi: 10.1190/1.1441329. [Link]

Ogata, Y. and K. Abe, 1991: Some statistical features of the long-term variation of the global and regional seismic activity. *Int. Stat. Rev.*, **59**, 139-161, doi: 10.2307/1403440. [Link]

Okubo, P. G. and K. Aki, 1987: Fractal geometry in the San Andreas fault system. *J. Geophys. Res.*, **92**, 345-355, doi: 10.1029/jb092ib01p00345. [Link]

Papadopoulos, G. A. and V. Dedousis, 1992: Fractal approach of the temporal earthquake distribution in the Hellenic arc-trench system. *Pure Appl. Geophys.*, **139**, 269-276, doi: 10.1007/bf00876331. [Link]

Pyrak-Nolte, L. J. and D. D. Nolte, 1995: Wavelet analysis of velocity dispersion of elastic interface waves propagating along a fracture. *Geophys. Res. Lett.*, **22**, 1329-1332, doi: 10.1029/95GL01323. [Link]

Richter, C. F., 1958: Elementary Seismology. Freeman, San Francisco, 768 pp.

Royden, L. H., B. C. Burchfiel, and R. D. van der Hilst, 2008: The geological evolution of the Tibetan Plateau. *Science*, **321**, 1054-1058, doi: 10.1126/science.1155371. [Link]

Smalley, R. F., J.-L. Chatelan, D. L. Turcotte, and R. Prevot, 1987: A fractal approach to the clustering of earthquakes: applications to the seismicity of the New Hebrides. *Bull. Seismol. Soc. Am.*, **77**, 1368-1381.

Takayasu, H., 1990: Fractals in the Physical Sciences. Manchester Univ. Press, Manchester, 176 pp.

Tan, T. K., J. Z. Zheng, J. Liu, and Y. Zou, 1987: Seismic patterns in Northern China and the characteristics of the epicentral distribution of the medium strong earthquakes before the large events. *Tectonophysics*, **138**, 45-53, doi: 10.1016/0040-1951(87)90064-3. [Link]

Tapponnier, P. and P. Molnar, 1977: Active faulting and tectonics in China. *J. Geophys. Res.*, **82**, 2905-2030, doi: 10.1029/jb082i020p02905. [Link]

Tapponnier, P., G. Peltzer, A. Y. L. Dain, R. Armijo, and P. Cobbold, 1982: Propagating extrusion tectonics in Asia: New insights from simple experiments with plasticine. *Geology*, **10**, 611-616, doi: 10.1130/0091-7613(1982)10<611:PETIAN>2.0.CO;2. [Link]

Tapponnier, P., Z. Xu, F. Roger, H. Meyer, N. Arnaud, G. Wittlinger, and J. Yang, 2001: Oblique stepwise rise and growth of the Tibet Plateau. *Science*, **294**, 1671-1677, doi: 10.1126/science.105978. [Link]

Torrence, C. and G. P. Compo, 1998: A practical guide to wavelet analysis. *Bull. Am. Meteorol. Soc.*, **79**, 61-78, doi: 10.1175/1520-0477(1998)079<0061:APGTWA>2.0.CO;2. [Link]

Turcotte, D. L., 1986a: Fractals and fragmentation. *J. Geophys. Res.*, **91**, 1921-1926, doi: 10.1029/JB091iB02p01921. [Link]

Turcotte, D. L., 1986b: A fractal model for crustal deformation. *Tectonophysics*, **132**, 261-269, doi: 10.1016/0040-1951(86)90036-3. [Link]

Turcotte, D. L., 1989: Fractals in geology and geophysics. *Pure Appl. Geophys.*, **131**, 171-196, doi: 10.1007/BF00874486. [Link]

Turcotte, D. L., 1997: Fractals and Chaos in Geology and Geophysics. Cambridge Univ. Press, Cambridge, U.K., 398 pp.

Wang, J. H., 1988: *b* values of shallow earthquakes in Taiwan. *Bull. Seismol. Soc. Am.*, **78**, 1243-1254.

Wang, J. H., 1991: A note on the correlation between b-value and fractal dimension from synthetic seismicity. *Terr. Atmos. Ocean. Sci.*, **2**, 317-329, doi: 10.3319/TAO.1991.2.4.317(T). [Link]

Wang, J. H., 1995: Effect of seismic coupling on the scaling of seismicity. *Geophys. J. Int.*, **121**, 475-488, doi: 10.1111/j.1365-246x.1995.tb05727.x. [Link]

Wang, J. H., 1996a: Multifractal measures of time series of M$_s$≥7 earthquakes in Taiwan. *J. Geol. Soc. China*, **39**, 117-123.

Wang, J. H., 1996b: Velocity-weakening friction as a factor in controlling the frequency- magnitude relation of earthquakes. *Bull. Seismol. Soc. Am.*, **86**, 701-713.

Wang, J. H., 2008: One-dimensional dynamical modeling of earthquakes: A review. *Terr. Atmos. Ocean. Sci.*, **19**, 183-203, doi: 10.3319/TAO.2008.19.3.183(T). [Link]

Wang, J. H., 2013: Memory effect in M≥6 earthquakes of South-North Seismic Belt, Mainland China. *J. Seismol.*, **17**, 913-924, doi: 10.1007/s10950-013-9361-8. [Link]

Wang, J. H. and H. C. Kuo, 1995: A catalogue of M$_s$≥7 Taiwan earthquakes (1900–1994). *J. Geol. Soc. China*, **38**, 95-106.

Wang, J. H. and C. W. Lee, 1995: Fractal characterization of an earthquake sequence. *Phys. Stat. Mech. Appl.*, **221**, 152-158, doi: 10.1016/0378-4371(95)00270-H. [Link]

Wang, J. H. and C. W. Lee, 1997: Multifractal measures of time series of earthquakes. *J. Phys. Earth*, **45**, 331-345, doi: 10.4294/jpe1952.45.331. [Link]

Wang, J. H. and W. H. Lin, 1993: A fractal analysis of earthquakes in west Taiwan. *Terr. Atmos. Ocean. Sci.*, **4**, 457-462, doi: 10.3319/TAO.1993.4.4.457(A). [Link]

Wang, J. H. and H. Y. Shen, 1999: Multifractal measures of epicentral distribution of M^{3}6 earthquakes in the north-south seismic belt of Mainland China. *J. Geol. Soc. China*, **42**, 631-637.

Wang, J. H., K. C. Chen, P. L. Leu, and C. H. Chang, 2015: b-Values Observations in Taiwan: A Review. *Terr. Atmos. Ocean. Sci.*, **26**, 475-492, doi: 10.3319/TAO.2015.04.28.01(T). [Link]

Wang, Z. and T. J. Zhong, 1987: Study on the sequential activity and consecutive strong earthquakes in mainland China. *Phys. Earth Planet. Inter.*, **46**, 343-356, doi: 10.1016/0031-9201(87)90089-6. [Link]

Xu, S. and P. Shen, 1981: Seismicity patterns in China. In: Simpson, D. W. and P. G. Richards (Eds.), Earthquake Prediction - An International Review, Maurice Ewing Series 4, AGU, 117-125, doi: 10.1029/ME004p0117. [Link]

YSB (Yunnan Seismological Bureau), 1998: The 1996 Lijian Earthquake in Yunnan, China. Seismology Press, 188 pp.

Zhang, Y., W. P. Feng, L. S. Xu, C. H. Zhou, and Y. T. Chen, 2009: Spatio-temporal rupture process of the 2008 great Wenchuan earthquake. *Sci. China Ser. D*, **52**, 145-154, doi: 10.1007/s11430-008-0148-7. [Link]

APPENDIX: EARTHQUAKE DATA IN USE

Table A1. The M ≥ 6 earthquakes in the South-North Seismic.

No	Date	Lat. (°N)	Long. (°E)	M	No	Date	Lat. (°N)	Long. (°E)	M	No	Date	Lat. (°N)	Long. (°E)	M
01	19010215	26.0	100.1	6.5	24	19300429	25.8	98.6	6.25	47	19400406	23.9	102.3	6.0
02	19040830	31.0	101.1	7.0	25	19300515	26.8	103.0	6.0	48	19410516	23.6	99.4	7.0
03	19090511	24.4	103.0	6.0	26	19300714	38.1	98.2	6.5	49	19410612	30.4	102.2	6.0
04	19090511	24.4	103.0	6.5	27	19300922	25.8	98.4	6.5	50	19411008	31.7	102.3	6.0
05	191308--	28.7	102.2	6.0	28	19300926	25.3	98.9	6.0	51	19411031	25.4	98.4	6.25
06	19131221	24.2	102.5	7.0	29	19301202	25.8	98.3	6.0	52	19411216	22.7	99.9	7.0
07	19170731	28.0	104.0	6.75	30	19310725	25.5	98.5	6.0	53	19420201	23.1	100.3	6.75
08	19190529	31.0	101.1	6.25	31	19320307	30.1	101.8	6.0	54	19470317	33.3	99.5	7.7
09	19190826	32.0	100.0	6.25	32	19330601	27.5	99.9	6.25	55	19480525	29.5	100.5	7.3
10	19201216	36.7	104.9	8.5	33	19330811	25.9	98.4	6.5	56	19480627	26.4	99.7	6.25
11	19210412	35.8	106.2	6.5	34	19330825	31.9	103.4	7.5	57	19490615	33.3	100.0	6.0
12	192105--	29.0	98.5	6.5	35	19340112	23.7	102.7	6.0	58	19500203	21.7	100.1	7.0
13	19230324	31.5	101.0	7.3	36	19340119	25.9	98.3	6.0	59	19500203	22.1	99.9	6.75
14	19230701	22.0	100.5	6.5	37	19350726	33.3	101.1	6.0	60	19511221	26.7	100.0	6.25
15	19231020	30.0	99.0	6.5	38	19351218	28.7	103.6	6.0	61	19520619	22.7	99.8	6.5
16	19250316	25.7	100.4	7.0	39	19351219	29.1	103.3	6.0	62	19520930	28.3	102.2	6.75
17	19251015	26.9	100.1	6.0	40	19360207	35.4	103.4	6.75	63	19521101	33.3	101.0	6.0
18	19270315	26.0	103.0	6.0	41	19360427	28.9	103.6	6.75	64	19540211	39.0	101.3	7.3
19	19270316	38.2	98.2	6.0	42	19360516	28.5	103.6	6.75	65	19540731	38.8	104.2	7.0
20	19270523	37.7	102.2	8.0	43	19360801	34.2	105.7	6.0	66	19550322	25.9	98.4	6.0
21	19290322	24.0	103.0	6.0	44	19380314	32.3	103.6	6.0	67	19550414	30.0	101.8	7.5
22	19291017	25.8	98.7	6.5	45	19380514	21.7	99.5	6.0	68	19550607	26.5	101.1	6.0
23	19300428	32.0	100.0	6.0	46	19380823	37.4	98.5	6.0	69	19550923	26.6	101.8	6.75

Table A1. (Continued)

No	Date	Lat. (°N)	Long. (°E)	M	No	Date	Lat. (°N)	Long. (°E)	M	No	Date	Lat. (°N)	Long. (°E)	M
70	19580208	31.5	104.0	6.2	87	19730816	23.1	101.2	6.3	103	19881106	23.4	99.6	7.1
71	19601109	32.7	103.7	6.75	88	19740511	28.2	104.1	7.1	104	19890416	30.0	99.4	6.7
72	19610627	21.7	99.8	6.0	89	19750115	29.4	101.9	6.2	105	19890425	29.7	99.4	6.7
73	19610624	25.2	101.2	6.2	90	19760529	24.5	99.0	7.3	106	19890503	30.0	99.4	6.4
74	19630423	25.8	99.5	6.0	91	19760529	24.6	98.7	7.4	107	19890922	31.5	102.6	6.6
75	19650703	22.4	101.6	6.1	92	19760816	32.6	104.1	7.2	108	19900426	36.1	100.3	6.9
76	19660205	26.1	103.1	6.5	93	19760823	32.5	104.3	7.2	109	19901020	37.1	103.5	6.2
77	19660213	26.1	103.1	6.2	94	19760923	39.9	106.4	6.2	110	19960203	27.3	100.3	6.6
78	19660928	27.5	100.1	6.4	95	19761107	27.6	101.1	6.7	111	20080512	31.0	103.3	7.9
79	19670830	31.6	100.3	6.8	96	19761213	27.4	101.0	6.4	112	20080512	31.2	103.6	6.1
80	19700105	24.2	102.7	7.7	97	19790315	23.2	101.1	6.8	113	20080525	32.6	105.4	6.1
81	19700207	23.08	101.03	6.2	98	19810124	31.0	101.2	6.9	114	20080805	32.8	105.5	6.0
82	19700224	30.6	103.3	6.2	99	19840424	22.1	99.2	6.0	115	20080830	26.2	101.9	6.0
83	19710324	35.5	98.1	6.3	100	19850418	25.9	102.9	6.3	116	20130420	30.3	102.9	6.6
84	19710428	23.0	101.1	6.7	101	19860826	37.7	101.5	6.4	117	20140803	27.2	103.4	6.2
85	19730206	31.3	100.7	7.6	102	19881106	22.8	99.7	7.5	118	20141007	23.4	100.5	6.1
86	19730811	32.9	104.1	6.5										